

## DIFFUSION OF H<sub>2</sub>O AND I<sup>−</sup> IN EXPANDABLE MICA AND MONTMORILLONITE GELS: CONTRIBUTION OF BOUND H<sub>2</sub>O

YOSHITO NAKASHIMA\*

Exploration Geophysics Research Group, National Institute of Advanced Industrial Science and Technology, Central 7,  
Higashi 1-1-1, Tsukuba, Ibaraki 305-8567, Japan

**Abstract**—Self-diffusion coefficients of H<sub>2</sub>O molecules in water-rich gels of Na-rich expandable mica synthesized using natural talc were measured by pulsed-gradient spin-echo <sup>1</sup>H nuclear magnetic resonance (NMR), and the dependence on mica fraction (0.00–43.8 wt.%) and temperature (30.0–60.9°C) was examined. On the basis of the NMR results, the self-diffusion coefficient of H<sub>2</sub>O,  $D_{\text{water}}$ , in the gel can be expressed by  $\ln(D_{\text{water}}/D_0^{\text{water}}) = 1.64[\exp(-0.0588w) - 1]$ , where  $D_0^{\text{water}}$  is the self-diffusivity of bulk water at temperature and  $w$  is the weight fraction of the mica (wt.%). The activation energy of H<sub>2</sub>O diffusivity in mica gel is nearly equal to that in bulk water. These findings indicate that the normalized diffusivity,  $D_{\text{water}}/D_0^{\text{water}}$ , is independent of temperature. The diffusivity of I<sup>−</sup>,  $D_{\text{iodine}}$ , in the gels was examined by X-ray computed tomography (CT) at 22°C, and the influence of the mica fraction (0.00–24.8 wt.%) was studied to determine the contribution of bound H<sub>2</sub>O. The X-ray CT results show that the normalized I<sup>−</sup> diffusivity,  $D_{\text{iodine}}/D_0^{\text{iodine}}$ , obeys the above-mentioned phenomenological curve where  $D_0^{\text{iodine}}$  is the I<sup>−</sup> diffusivity in bulk water. I<sup>−</sup> is non-sorbing, and thus its diffusion is restricted only by the geometrical complexity of the pore structure of gels. Therefore, the effect of bound H<sub>2</sub>O molecules on average H<sub>2</sub>O diffusivity is negligible for  $w < 24.8$  wt.%. Diffusivity is governed by free or unbound H<sub>2</sub>O molecules diffusing in the geometrically complex and tortuous pore structure of mica-mineral grains. This is a result of the large population of unbound H<sub>2</sub>O far from the grain surface compared to the small population of bound H<sub>2</sub>O near the grain surface. The diffusion of I<sup>−</sup> ions in montmorillonite gels was examined by X-ray CT for  $w < 16.7$  wt.% montmorillonite. The normalized iodine diffusivity,  $(D_{\text{iodine}}/D_0^{\text{iodine}})$  obtained is in reasonably close agreement with the literature data for the normalized diffusivity of H<sub>2</sub>O and is similar to the master curve of expandable mica. Therefore, bound H<sub>2</sub>O molecules near negatively charged clay surfaces do not play a major role in the H<sub>2</sub>O diffusivity for water-rich montmorillonite gels.

**Key Words**—Diffusion, Expandable Mica, H<sub>2</sub>O, Iodine, Montmorillonite, Nuclear Magnetic Resonance (NMR), X-ray Computed Tomography (CT).

### INTRODUCTION

H<sub>2</sub>O diffusivity is a fundamental transport property for systems of H<sub>2</sub>O and clay minerals. Many studies have been published on H<sub>2</sub>O diffusivity in clays and clay minerals, and it has been shown that the diffusivity in such systems is lower than that in bulk water (*e.g.* Fripiat *et al.*, 1984; Tuck *et al.*, 1985; McBride, 1994; Yu and Neretnieks, 1997). Two mechanisms have been proposed for the low diffusivity in porous media: the geometrical complexity of the porous structure; the existence of bound or less mobile H<sub>2</sub>O near the solid surface. One of the most important issues that needs to be clarified is the contribution of bound H<sub>2</sub>O molecules to the average diffusivity of the system. Cebula *et al.* (1981), McBride (1994), Chang *et al.* (1995) and Ichikawa *et al.* (1999) predicted that the contribution is negligible for water-rich clay gels. However, the existence or predominance of either mechanism has yet to be verified quantitatively. This has been addressed experimentally in the present

study by measuring the diffusivity of H<sub>2</sub>O and I<sup>−</sup> in water-rich gels. The I<sup>−</sup> ion is non-sorbing in water-rich gels (*e.g.* Madsen, 1998) and is not affected by adsorption which reduces diffusivity. The success of such an approach (*e.g.* S. Nakashima, 1995; Y. Nakashima, 2000a) indicates that I<sup>−</sup> diffusion experiments are appropriate for probing the geometrical complexity of water-saturated porous media. Theoretically the contribution of bound H<sub>2</sub>O to H<sub>2</sub>O diffusivity can be calculated by subtracting the geometrical effects obtained by the I<sup>−</sup> experiments from the measured H<sub>2</sub>O diffusivity. Hence the coordinated study of H<sub>2</sub>O diffusivity and I<sup>−</sup> diffusivity is expected to allow differentiation of the effects of geometrical complexity and bound H<sub>2</sub>O. This technique was applied in this study to two expandable clay minerals (synthetic mica and natural montmorillonite).

The self-diffusion coefficients of H<sub>2</sub>O molecules in mica gels were measured using pulsed-field-gradient <sup>1</sup>H nuclear magnetic resonance (NMR). Other techniques, such as molecular dynamics simulation and neutron scattering are not applicable because the characteristic diffusion distance is too small (typically several nm), making it impossible to measure the long diffusion

\* E-mail address of corresponding author:  
nakashima.yoshito@aist.go.jp

across pores (typically several hundred nm in diameter). In contrast, NMR is capable of following diffusion distances of up to a few hundred  $\mu\text{m}$  with high precision (*e.g.* Latour *et al.*, 1995). Hence, NMR is very suited to obtaining diffusion data for  $\text{H}_2\text{O}$  travelling in the complex pore structure of clay gels (Fripiat *et al.*, 1984; Nakashima *et al.*, 1999; Nakashima, 2000b, 2001a,b). This technique was used in this study to examine the effect of the mica weight fraction and temperature on the self-diffusion coefficients of  $^1\text{H}_2\text{O}$  molecules in these gels.

The diffusion coefficients of  $\text{I}^-$  in gels were measured by X-ray computed tomography (CT). X-ray CT can be used to visualize non-destructively the spatial distribution of heavy elements (*e.g.* iodine) with a reasonable resolution ( $\sim 1 \text{ mm}$ ), in a short time ( $\sim 10 \text{ s}$ ), and with high precision ( $\sim 13 \text{ bit}$ ). Thus it is ideal for imaging the diffusive migration of heavy ions, as first demonstrated by Nakashima (2000a). This technique was used in the present study to probe the geometrical tortuosity of the pore structure of gels.

## EXPERIMENTAL METHOD

### Sample description

Two expandable clay minerals were used: synthetic mica and natural montmorillonite. The Na-rich expandable mica sample is a synthetic powder ME-100® by CO-OP Chemical Co., Ltd. (Tokyo, Japan). ME-100® is produced from natural talc and  $\text{Na}_2\text{SiF}_6$  (Tateyama *et al.*, 1992). The ideal formula is  $\text{Na}_{2+2x}\text{Mg}_{3-y}(\text{Si}_{4-x}\text{Mg}_x)\text{O}_{10}(\text{F},\text{OH})_2$  for  $0 < x, y < 0.5$  (Furusawa, 1997) and the analyzed chemical composition (wt.%) is: Si, 26.5; Al, 0.2; Fe, 0.1; Mg, 15.6; Na, 4.1; F, 3.8. The weight loss of the powder sample was 2.5 wt.% at  $110^\circ\text{C}$ . The average grain diameter is  $5 \mu\text{m}$  and the grain density is  $2.6 \text{ g/cm}^3$ . The synthetic mica expands by incorporating  $\text{H}_2\text{O}$  molecules into the silicate sheets to form water-rich gel. This Mn- and Fe-poor synthetic sample allows us to perform high-precision NMR experiments without degradation due to the presence of paramagnetic impurities which shorten the relaxation times of protons.

The Na-rich montmorillonite is from the Tsukinuno Mine, Yamagata, Japan and is a reference sample (JCSS3101) from the Japan Clay Science Society (available at URL = <http://wwwsoc.nii.ac.jp/cssj2/index.html>). The JCSS3101 sample contains 99 wt.% montmorillonite, 0.5 wt.% quartz and 0.5 wt.% calcite. The chemical composition has been described in detail by Nakashima *et al.* (1999) and Nakashima (2001a). The loss on heating of the JCSS3101 powder sample was 7.5 wt.% at  $110^\circ\text{C}$ . The average grain diameter was 800 nm (Monma *et al.*, 1997).

### PGSE NMR experiments

By adding deionized water to the powder sample, 13 gel samples of the expandable mica (ranging from 8.75

to 43.8 wt.% mica) were prepared. Samples of only a few wt.% mica were not examined because the preparation of homogeneous gels failed owing to the segregation of mica and bulk water. The self-diffusion coefficient in bulk water (deionized water) was also measured to evaluate the accuracy of the NMR data. Relaxation times ( $T_1$ , spin-lattice relaxation time, and  $T_2$ , spin-spin relaxation time) for protons associated with  $\text{H}_2\text{O}$  in the 13 gel samples and deionized water were measured at  $39.8^\circ\text{C}$ . The bulk densities,  $\rho_{\text{bulk}}$ , of the 14 samples at  $25^\circ\text{C}$  were obtained by weighing samples of a known volume.

Self-diffusion coefficients were calculated by measuring the decrease in NMR signal intensity with increasing magnetic field gradients (Stejskal and Tanner, 1965). In pulsed-gradient spin-echo (PGSE) NMR, the NMR spin-echo signal intensity,  $I$ , is given by:

$$I/I_0 = \exp(-bD^{\text{water}}) \quad (1)$$

where

$$b = (\gamma G \delta)^2 (\Delta - \delta/3) \quad (2)$$

The quantity  $I_0$  is the signal intensity without pulsed field gradients,  $\gamma$  is the gyromagnetic ratio of a proton ( $2.675 \times 10^8 \text{ rad/Ts}$ ),  $G$  is the strength of the gradient pulses,  $\delta$  is the duration of the field gradient pulses,  $\Delta$  is the interval between two gradient pulses (characteristic diffusion time of  $\text{H}_2\text{O}$  molecules), and  $D^{\text{water}}$  is the self-diffusion coefficient of  $\text{H}_2\text{O}$  (*e.g.* Johnson, 1996).

The PGSE NMR measurements were performed using a NMS120 proton spectrometer (Bruker, Karlsruhe, Germany) at a resonant frequency of 20 MHz. Each sample (volume,  $1 \text{ cm}^3$ ) was placed in a separate glass tube (outside diameter, 10 mm). The pulse parameters were as follows:  $\delta = 0.7 \text{ ms}$ , echo time  $T_E = 28 \text{ ms}$ ,  $\Delta = 14 \text{ ms}$ ,  $90^\circ$  pulse length  $3.0 \mu\text{s}$ , and 16 stacked echo signals. The repetition time of the pulse sequence,  $T_R$ , was taken as  $T_R = 5 T_1$  to meet the full relaxation condition. About 10 values of  $G$  (from 0 to  $2.1 \text{ T/m}$ ) were used for a specific mica fraction and temperature to measure the dependence of  $I/I_0$  on  $b$ . The  $D^{\text{water}}$  value was then calculated by performing a regression analysis of the data sets ( $I/I_0, b$ ) using equations 1 and 2. The experiments were performed at atmospheric pressure and no pressure vessel was used. Four temperatures ( $30.0, 39.8, 50.7$  and  $60.9^\circ\text{C}$ ) were chosen to calculate the activation energy for the diffusion process.

Diffusing  $\text{H}_2\text{O}$  molecules go around impermeable obstacles such as mica grains in porous gels. Therefore, the random-walk trajectory of  $\text{H}_2\text{O}$  is likely to be restricted by the obstacles, and is termed ‘the restricted diffusion regime’. The condition of the regime is given by  $\Delta \gg d^2/6D^{\text{water}}$  where  $d$  is the average pore diameter of the gel (*e.g.* Callaghan, 1991). The physical meaning of this condition is that the characteristic diffusion time of  $\text{H}_2\text{O}$  ( $\Delta$ ) is much longer than the time required for diffusing  $\text{H}_2\text{O}$  to traverse a single pore of size  $d$ .

( $d^2/6D_{\text{water}}$ ). The regime is characterized by the  $\Delta$  independence of  $D_{\text{water}}$  in terms of diffusivity. Hence, large- $\Delta$  experiments ( $\Delta = 120$  ms) were also performed for some samples to confirm that the measured  $H_2O$  diffusivity occurred under this regime. No NMR experiments were performed for montmorillonite gels because NMR data on JCSS3101 were published by Nakashima (2001a).

### X-ray CT experiments

X-ray CT is a radiological imaging system that is used in geology to image minerals and rocks (e.g. Nakashima, *et al.*, 1997; Ohtani *et al.*, 2001). The principle of this imaging technique is described by Wellington and Vinegar (1987), Denison *et al.* (1997), Diliu (1999), and van Geet *et al.* (2000), and involves measuring the attenuation of two-dimensional fan-beams of X-rays penetrating a sample from various directions using an array of detectors. A two-dimensional 16-bit TIFF image of the X-ray linear absorption coefficient (LAC) of the sample is reconstructed using the detector data. The LAC itself is related to the density and atomic number of the sample (e.g. MacGillavry and Rieck, 1962; URL = <http://physics.nist.gov/PhysRefData/Xcom/Text/XCOM.html>). For the medical X-ray CT scanner used in this study, the following empirical relation was determined:

$$\text{LAC} \propto cZ^{3.2} \quad (3)$$

where  $c$  is the molar concentration of the substance and  $Z$  is its atomic number (Nakashima, 2000a). Because the image intensity (*i.e.* LAC) is sensitive to  $Z$ , X-ray CT allows us to visualize where elements with high atomic numbers concentrate. This is the basis for the diffusion measurement of heavy ions by X-ray CT.

The measurement of  $I^-$  diffusion in mica gels by X-ray CT was performed according to the method of Nakashima (2000a). Samples of mica gels were prepared by adding deionized water to the powder sample followed by centrifugation. The gel was then transferred to a plastic cylindrical container to prevent water evaporation during the experiment. The weight fraction of mica was varied between 7.69 and 24.8 wt.% mica, and montmorillonite was varied between 3.24 and 16.7 wt.%. Samples with higher fractions were not examined owing to the presence of undesirable air-filled voids (several mm in size) in the gels, which reduces the signal-to-noise ratio of the CT images. The  $I^-$  diffusion in bulk water was also measured to evaluate the accuracy of the X-ray CT data. We chose KI as an iodine-bearing substance, and hence  $K^+$  ions as well as  $I^-$  ions diffused in the experiments. However, the contribution of  $K^+$  to the CT image is negligible owing to its low atomic number (Nakashima, 2000a). Therefore, only the migration of  $I^-$  ions was effectively imaged.

The third-generation medical X-ray CT scanner, W2000 (Hitachi Medical Co., Tokyo, Japan) of the

Geological Survey of Japan was used. The imaging conditions were as follows. The slice thickness (thickness of the X-ray fan-beam) was 2 mm and the in-plane resolution of the images obtained was 0.31 mm. Thus the resolution or voxel (volume element) dimension was  $0.31 \times 0.31 \times 2$  mm<sup>3</sup>. The original image consisted of  $512 \times 512$  voxels and the field of view was  $512 \times 0.31$  mm = 16 cm. A target (Mo-W alloy) in an X-ray tube was bombarded by electrons accelerated at 120 kV with a 150 mA current. The X-ray exposure time (time for a 360° rotation of the X-ray tube) was 4 s. A special image-reconstruction method (Olson *et al.*, 1981) was used to reduce the effect of beam-hardening derived from the polychromatic photon energy of the X-ray. All imaging experiments were performed at 22°C.

The one-dimensional transient diffusion of  $I^-$  ions was imaged by X-ray CT. Filter paper was immersed in aqueous KI solution (36 wt.%) and then placed on the gel, and the downward diffusive migration of  $I^-$  was imaged by X-ray CT. The  $I^-$  diffusion in bulk water was measured by injecting a dense KI solution into the bottom of the plastic container using a syringe and imaging the upward diffusion (Nakashima, 2000a). The color of the KI solution remained transparent throughout the experiments, implying that the undesirable formation of  $I_3^-$  (yellow) was negligible (Kita *et al.*, 1989). The degree of X-ray attenuation increases linearly with the molar concentration of iodine. By convention, the LACs were converted into non-dimensional CT numbers (in Hounsfield units) normalized against the LAC of pure water (e.g. Diliu, 1999). Hence the molar concentration of  $I^-$  in a voxel of an image increases linearly with the CT number or voxel intensity. A part of each original image (16 × 16 cm<sup>2</sup> in size) was extracted to calculate diffusion coefficients. The exact solution of one-dimensional diffusion in an homogeneous semi-infinite medium [0, ∞] for the initial condition that all diffusants are concentrated at  $x = 0$  is given by:

$$c(x, t) \supset \frac{\int_0^\infty c(x, 0) dx}{\sqrt{\pi D_{\text{iodine}} t}} \exp\left(-\frac{x^2}{4D_{\text{iodine}} t}\right) \quad (4)$$

where  $c$  is the molar concentration of  $I^-$ ,  $x$  is the distance from the origin,  $t$  is the elapsed time and  $D_{\text{iodine}}$  is the diffusion coefficient of  $I^-$  (e.g. Crank, 1975). Line profiles of  $c$  along the  $x$  axis were extracted from the CT images and fitted to equation 4 by a least-squares method to find  $D_{\text{iodine}}$ .

## RESULTS AND DISCUSSION

### Expandable mica gel

The  $D_{\text{water}}$  value can be qualitatively discussed in terms of Figure 1 which shows that  $T_1$  and  $T_2$  decrease as the mica fraction increases. The principal mechanism for the spin relaxation in porous media is the collision of diffusing  $H_2O$  molecules with minerals (Kleinberg and

Vinegar, 1996). The smaller  $T_1$  and  $T_2$  implies a higher collision-frequency attributable to the smaller pore-size of the gel or the denser packing of mica grains. Smaller pore-sizes give lower values of  $D^{\text{water}}$  because the densely packed grains are obstacles for the diffusing water molecules. From Figure 1 it can be suggested that  $D^{\text{water}}$  decreases with increasing mica fraction. This hypothesis was verified quantitatively by the PGSE NMR experiments.

Examples of  $b$ -dependent echo intensities are shown for selected mica samples in Figure 2. The variation in the spin-echo signal with the strength of the field gradient can be clearly seen. The slope of each regression line represents the self-diffusion coefficient of  $\text{H}_2\text{O}$ ,  $D^{\text{water}}$ . The accuracy of the PGSE NMR experiments can be discussed using the diffusion coefficient for bulk water. Mills (1973) produced very reliable values for diffusion in bulk water: the self-diffusivity of bulk water is  $2.30 \times 10^{-9} \text{ m}^2/\text{s}$  at  $25.0^\circ\text{C}$  and the activation energy of the diffusion is  $17.6 \text{ kJ/mol}$ . Thus, the predicted bulk-water diffusivities at other temperatures are given as  $2.59 \times 10^{-9} \text{ m}^2/\text{s}$  at  $30.0^\circ\text{C}$ ,  $3.22 \times 10^{-9} \text{ m}^2/\text{s}$  at  $39.8^\circ\text{C}$ ,  $4.04 \times 10^{-9} \text{ m}^2/\text{s}$  at  $50.7^\circ\text{C}$ , and  $4.93 \times 10^{-9} \text{ m}^2/\text{s}$  at  $60.9^\circ\text{C}$ . The measured values were  $2.55 \times 10^{-9}$ ,  $3.27 \times 10^{-9}$ ,  $4.11 \times 10^{-9}$ , and  $5.04 \times 10^{-9} \text{ m}^2/\text{s}$ , respectively (Table 1), which is in good agreement with the predictions, confirming the

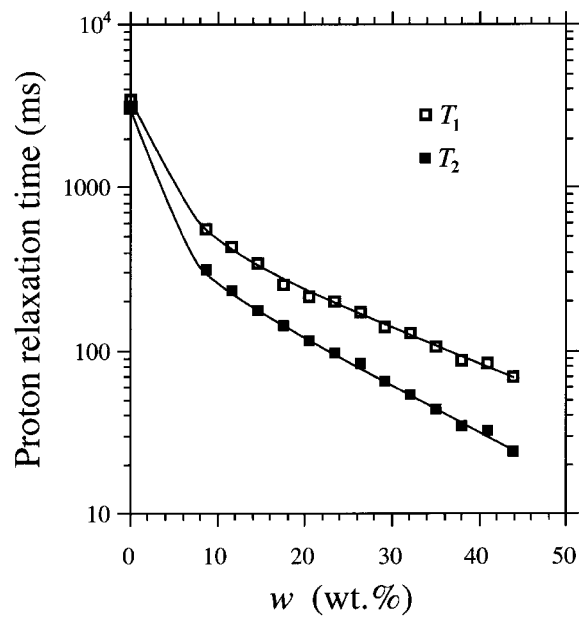


Figure 1. Relaxation times of protons in expandable mica gels at 20 MHz and  $39.8^\circ\text{C}$  vs. mica fraction,  $w$  (data from Table 1).  $T_1$  and  $T_2$  were measured by the inversion recovery method and the Carr-Purcell-Meiboom-Gill (CPMG) method, respectively. The  $90^\circ$  to  $180^\circ$  pulse separation was 0.3 ms for the CPMG method. The solid lines are approximated trend lines.

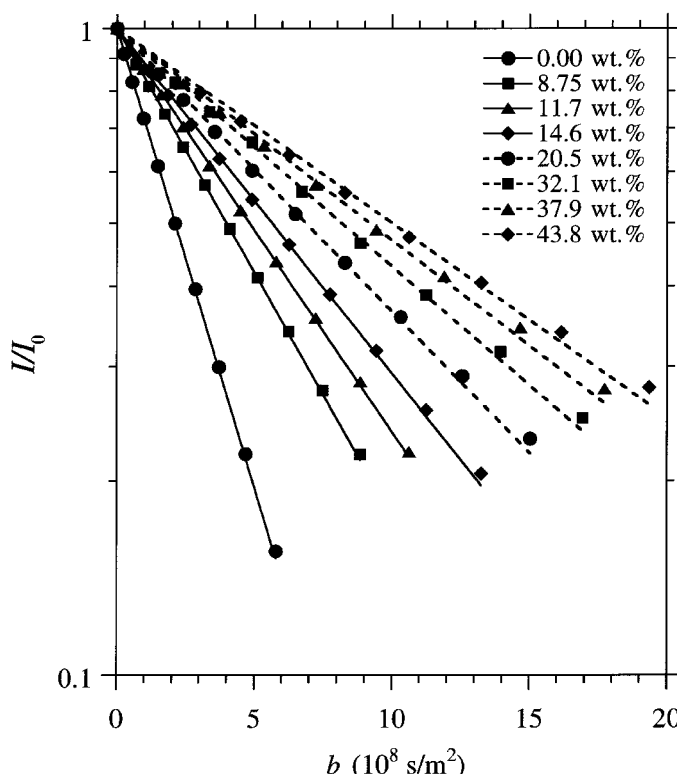


Figure 2. NMR signal intensities vs.  $b$  factor at  $39.8^\circ\text{C}$  for eight samples. Each mica fraction is indicated. Data points are fitted to equation 1 by a least-squares method. Note that higher  $D^{\text{water}}$  yields a higher slope.

Table 1. Results of the NMR experiments of expandable mica gels ( $\Delta = 14$  ms). The water fraction (wt.%) is  $100 - w$  and includes pre-existing  $H_2O$  (weight loss of 2.5 wt.% at  $110^\circ C$ ) of the mica powder.

| $w$<br>(wt.%) | $\rho_{\text{bulk}}$<br>$25^\circ C$<br>(g/ml) | $T_1$                  | $T_2$                  | $D$<br>$30.0^\circ C$            | $D$<br>$39.8^\circ C$            | $D$<br>$50.7^\circ C$            | $D$<br>$60.9^\circ C$            | $E$<br>(kJ/mol) |
|---------------|--|------------------------|------------------------|----------------------------------|----------------------------------|----------------------------------|----------------------------------|-----------------|
|               |  | $39.8^\circ C$<br>(ms) | $39.8^\circ C$<br>(ms) | $(10^{-9} \text{ m}^2/\text{s})$ | $(10^{-9} \text{ m}^2/\text{s})$ | $(10^{-9} \text{ m}^2/\text{s})$ | $(10^{-9} \text{ m}^2/\text{s})$ |                 |
| 0.00          | 1.0  | 3458                   | 3084                   | 2.55                             | 3.27                             | 4.11                             | 5.04                             | 17.8            |
| 8.75          | 1.1  | 561                    | 311                    | 1.37                             | 1.74                             | 2.19                             | 2.64                             | 17.4            |
| 11.7          | 1.1  | 431                    | 231                    | 1.14                             | 1.44                             | 1.84                             | 2.23                             | 17.8            |
| 14.6          | 1.2  | 341                    | 176                    | 0.979                            | 1.23                             | 1.57                             | 1.93                             | 18.0            |
| 17.5          | 1.2  | 254                    | 144                    | 0.880                            | 1.10                             | 1.40                             | 1.69                             | 17.3            |
| 20.5          | 1.2  | 216                    | 116                    | 0.813                            | 1.01                             | 1.28                             | 1.55                             | 17.2            |
| 23.4          | 1.2  | 199                    | 98.5                   | 0.759                            | 0.938                            | 1.17                             | 1.43                             | 16.8            |
| 26.3          | 1.2  | 174                    | 84.6                   | 0.737                            | 0.915                            | 1.14                             | 1.39                             | 16.7            |
| 29.1          | 1.3  | 141                    | 64.7                   | 0.686                            | 0.857                            | 1.07                             | 1.29                             | 16.6            |
| 32.1          | 1.3  | 129                    | 54.3                   | 0.679                            | 0.848                            | 1.07                             | 1.28                             | 16.8            |
| 35.1          | 1.3  | 106                    | 43.6                   | 0.666                            | 0.853                            | 1.03                             | 1.24                             | 16.6            |
| 37.9          | 1.4  | 88.6                   | 34.6                   | 0.619                            | 0.752                            | 0.947                            | 1.13                             | 16.1            |
| 40.9          | 1.4  | 83.9                   | 32.1                   | 0.585                            | 0.731                            | 0.883                            | 1.08                             | 16.4            |
| 43.8          | 1.4  | 69.6                   | 24.2                   | 0.582                            | 0.692                            | 0.845                            | 1.04                             | 16.0            |

accuracy of our measurements. The results of these bulk-water experiments suggest that the accuracy of the PGSE NMR experiments is near  $10^{-11} \text{ m}^2/\text{s}$ .

The restricted diffusion regime is characterized by the  $\Delta$ -independence of  $D_{\text{water}}$ . The diffusivity obtained in small- and large- $\Delta$  experiments was compared to confirm that the  $H_2O$  diffusivity was measured under this regime. For example, measured  $D_{\text{water}}$  values at  $39.8^\circ C$  for  $\Delta = 14$  ms were 1.44, 1.10 and  $0.938 \times 10^{-9} \text{ m}^2/\text{s}$  for  $w = 11.7$ , 17.5 and 23.4 wt.%, respectively (Table 1). The values for  $\Delta = 120$  ms were 1.48, 1.08 and  $0.921 \times 10^{-9} \text{ m}^2/\text{s}$ , respectively. These results are consistent within experimental error, suggesting that the present NMR experiments are conducted entirely in the restricted diffusion regime. The migration distance (root-mean-square displacement) of random walkers in three-dimensional space is given by  $(6\Delta D_{\text{water}})^{1/2}$  (e.g. Callaghan, 1991). Using  $D_{\text{water}} = 0.6 - 2.6 \times 10^{-9} \text{ m}^2/\text{s}$  (Table 1) and  $\Delta = 14$  ms,  $(6\Delta D_{\text{water}})^{1/2}$  falls within 7 to 15  $\mu\text{m}$ . This characteristic diffusion length in NMR experiments is several orders of magnitude longer than the measurable lengths in molecular-dynamic simulations and neutron-scattering experiments. This is why NMR is appropriate for probing the complexity of the pore structure. The average mica grain diameter is 5  $\mu\text{m}$ , which means that the mica-gel pore-size is as small as a few  $\mu\text{m}$  or less because the gel structure is constructed by the packing of fine grains. Thus, for example, if the pore-size is 1  $\mu\text{m}$  and  $(6\Delta D_{\text{water}})^{1/2} = 10 \mu\text{m}$ , the diffusivity measured by PGSE NMR is the diffusivity of  $H_2O$  molecules migrating through about  $10/1 = 10$  pores.

The  $H_2O$  self-diffusion coefficients,  $D_{\text{water}}$ , in the expandable mica gels are shown as a function of mica weight fraction (wt.%),  $w$ , for various temperatures in Figure 3 and Table 1. All  $D_{\text{water}}$  values in the gels are smaller than those in bulk water. At high  $w$ ,  $D_{\text{water}}$  is small because the  $H_2O$  mobility is strongly restricted by

the densely packed mineral grains. As  $w$  decreases, the density of obstacles (mica grains) for the random walk decreases, and thus  $H_2O$  mobility increases. For a water-rich sample, the  $H_2O$  molecules diffuse as if they were in bulk water, and  $D_{\text{water}}$  approaches the diffusivity of bulk water.

A phenomenological equation relating  $w$  to  $D_{\text{water}}$  is proposed as follows:

$$\ln(D_{\text{water}}/D_0^{\text{water}}) = \alpha [\exp(-\beta w) - 1] \quad (5)$$

where  $D_0^{\text{water}}$  is the diffusivity of bulk water at temperature, and  $\alpha$  and  $\beta$  are dimensionless constants. Equation 5 satisfies  $D_{\text{water}} = D_0^{\text{water}}$  at  $w = 0$  wt.%. The fitting of equation 5 to the data is shown in Figures 3a and 4. Figure 3a shows that  $\alpha$  and  $\beta$  are nearly independent of sample temperature. As a result, a single temperature-independent master curve, equation 5, was determined (Figure 4). Although the numerical constants,  $\alpha$  and  $\beta$  are slightly different, equation 5 for expandable mica is identical to that for montmorillonite (Nakashima, 2001a). The phenomenological equation for hectorite gels found by Nakashima (2000b),  $D_{\text{water}}/D_0^{\text{water}} = \exp(\alpha'w)$  where  $\alpha'$  is a dimensionless constant, is quite different. The reason why hectorite behaves differently is a problem to be solved in the future.

An Arrhenius plot of the diffusion data is shown in Figure 3b and the calculated activation energy,  $E$ , is listed in Table 1. The activation energy is calculated from

$$D_{\text{water}} = A \exp(-E/RT) \quad (6)$$

where  $A$  is a constant,  $R$  is the gas constant, and  $T$  is absolute temperature. The activation energy of bulk water (17.8 kJ/mol; Table 1) for  $30.0 - 60.9^\circ C$  is nearly equal to the result reported by Mills (1973) of 17.6 kJ/mol for the temperature range  $15 - 45^\circ C$ , suggesting that the NMR experiments were performed in a reliable manner. Whereas over a broader temperature

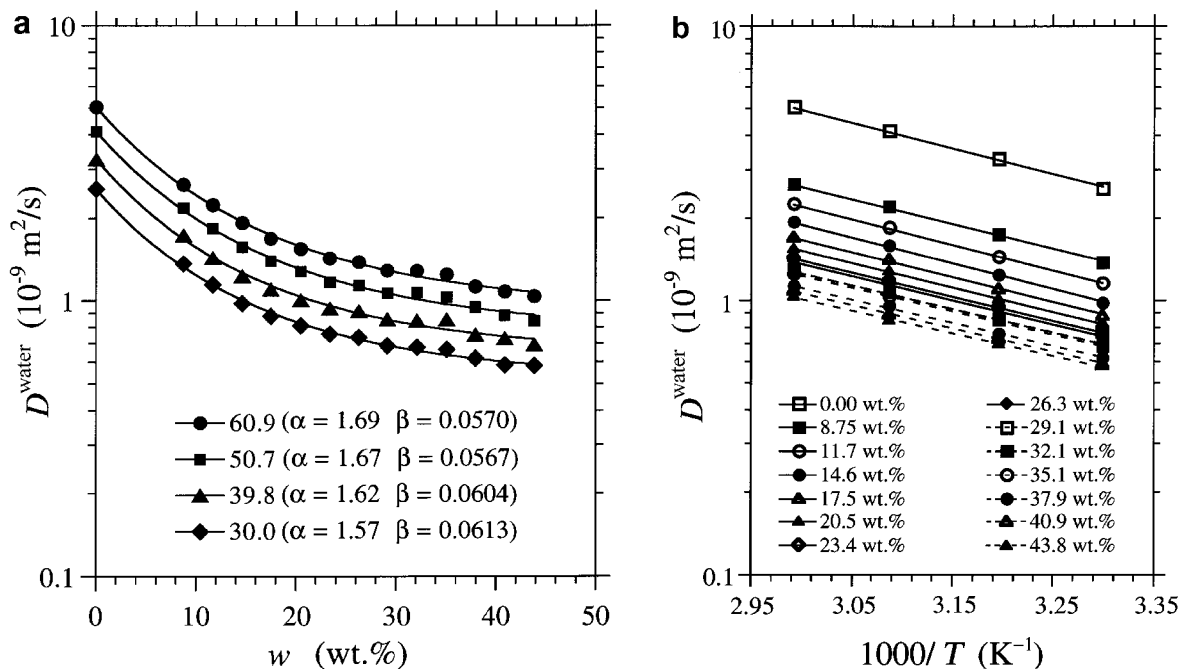


Figure 3. Self-diffusion coefficient of  $\text{H}_2\text{O}$ ,  $D_{\text{water}}$ , in expandable mica gel (data from Table 1). (a) Semi-log plot of  $D_{\text{water}}$  as a function of mica fraction,  $w$ , of the gel at various temperatures ( $^{\circ}\text{C}$ ). Parameters  $\alpha$  and  $\beta$  in equation 5 were fitted by a least-squares method. (b) Arrhenius plot of  $D_{\text{water}}$  for various mica fractions. Data points are fitted to equation 6 by a least-squares method.

range ( $2$ – $225^{\circ}\text{C}$ , Krynicki *et al.*, 1979;  $4$ – $55^{\circ}\text{C}$ , Fripiat *et al.*, 1984) bulk water and clay gel exhibit weakly non Arrhenius behavior, the Arrhenius fitting in Figure 3b appears reasonable, probably because of the narrow temperature range examined in the present study. Table 1 indicates that the activation energy for each

mica gel sample nearly equals the value for bulk water. The temperature-independence of  $\alpha$  and  $\beta$  in equation 5 is a consequence of this  $w$ -independence of  $E$ .

The results of the X-ray CT analysis of mica gels are listed in Table 2. It is possible to estimate the accuracy of the experiments using the  $\text{I}^-$  diffusivity in bulk water,  $D_0^{\text{iodine}}$ . On the basis of the  $\text{I}^-$  diffusivity in bulk water at  $0$ ,  $18$  and  $25^{\circ}\text{C}$  (Lerman, 1979),  $D_0^{\text{iodine}}$  at  $22^{\circ}\text{C}$  is estimated to be  $1.87 \times 10^{-9} \text{ m}^2/\text{s}$ . The measured diffusivity ( $1.88 \times 10^{-9} \text{ m}^2/\text{s}$ ) in Table 2 agrees well with this prediction. This confirms that the X-ray CT experiments were performed with a reasonable accuracy. Four snapshots of a diffusion cell (plastic container) are shown in Figure 5a. The gray-scale is common to all images. Filter paper saturated with dense KI solution

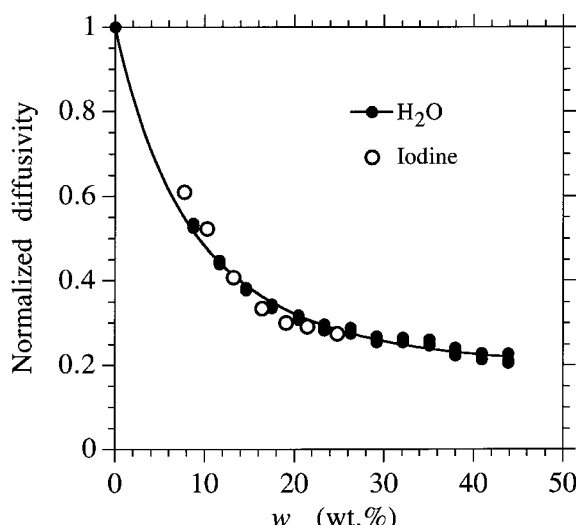


Figure 4. Normalized  $\text{H}_2\text{O}$  diffusivity,  $D_{\text{water}}/D_0$ , vs. mica fraction,  $w$  for  $30.0$ ,  $39.8$ ,  $50.7$  and  $60.9^{\circ}\text{C}$  (data identical to Figure 3). Data points are fitted to equation 5 by a least-squares method yielding  $\alpha = 1.64$  and  $\beta = 0.0588$ . Note that the normalized  $\text{H}_2\text{O}$  diffusivity is independent of temperature. The normalized iodine diffusivity,  $D_{\text{iodine}}/D_0^{\text{iodine}}$ , is also given (data from Table 2).

Table 2. Results of the X-ray CT experiments of expandable mica gel. The mica weight fraction (wt.%) is corrected using pre-existing  $\text{H}_2\text{O}$  (weight loss of  $2.5$  wt.% at  $110^{\circ}\text{C}$ ) of the mica powder.

| $w$<br>(wt.%) | $D_{\text{iodine}}$<br>$22^{\circ}\text{C}$<br>( $10^{-9} \text{ m}^2/\text{s}$ ) |
|---------------|---|
| 0.00          | 1.88  |
| 7.69          | 1.15  |
| 10.2          | 0.98  |
| 13.1          | 0.77  |
| 16.2          | 0.63  |
| 18.9          | 0.57  |
| 21.3          | 0.55  |
| 24.8          | 0.52  |

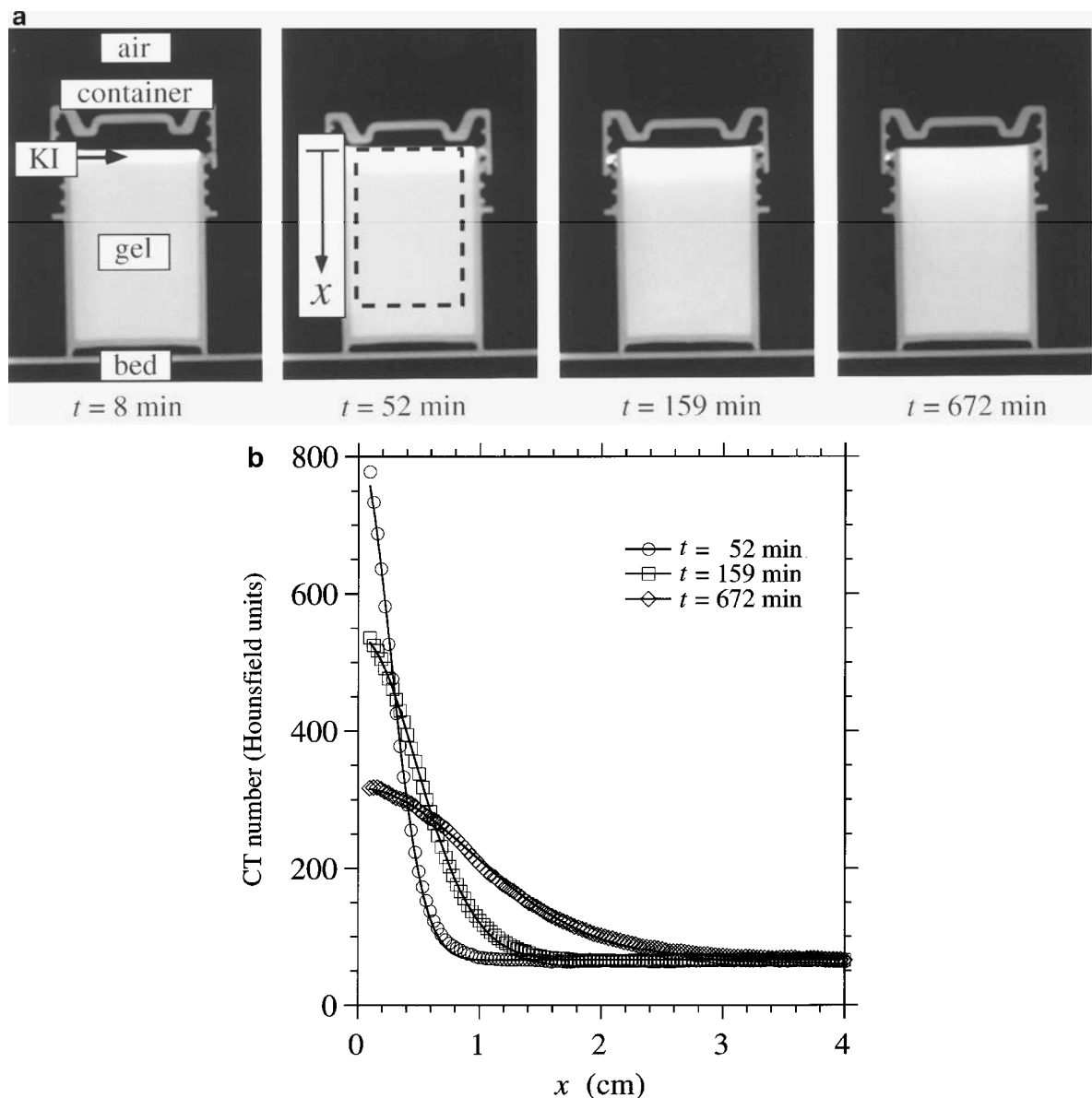


Figure 5.  $I^-$  diffusion in mica gel of  $w = 7.69 \text{ wt.\%}$ . (a) Two-dimensional X-ray CT images. The image dimensions are  $202 \times 287$  voxels or  $6.3 \times 9.0 \text{ cm}^2$ . (b) Profiles of CT numbers averaged over the dashed rectangle in part a.  $x$  is the distance from the filter paper. Equation 4, fitted by a least-squares method, is also shown.  $D^{iodine}$  is calculated to be  $1.13 \times 10^{-9} \text{ m}^2/\text{s}$  ( $t = 52 \text{ min}$ ),  $1.20 \times 10^{-9} \text{ m}^2/\text{s}$  ( $t = 159 \text{ min}$ ) and  $1.13 \times 10^{-9} \text{ m}^2/\text{s}$  ( $t = 672 \text{ min}$ ).

was placed on the gel at  $t = 0 \text{ s}$ . Figure 5a shows the resultant diffusive migration of iodine from the filter paper. The image is sensitive to the density and atomic number of the substance (equation 3). Therefore, iodine-rich voxels are brightest, voxels occupied by iodine-poor gel or plastic are dark, and the atmosphere is darkest. Profile averages were taken to improve the signal-to-noise ratio according to the method of Nakashima (2000a). By fitting the Gaussian curve to the profile,  $D_{iodine}$  was calculated (Figure 5b). Average values taken over a number of snapshots are given in Table 2.

There are two possible reasons for  $D_{water}/D_0^{water}$  being less than unity for gels: bound or less mobile  $H_2O$  molecules may occur near negatively charged mineral surfaces and the geometrical complexity of the pore structure of the gel through which  $H_2O$  molecules migrate according to a random walk. (1)  $H_2O$  molecules travel sufficiently long distances [ $(6\Delta D^{water})^{1/2} = 7\text{--}15 \mu\text{m}$ ] to be affected by the complex pore structure of the gel. Therefore, the complexity is a possible reason for the low  $H_2O$  diffusivity in mica gel. (2) Table 1 shows that  $E$  for gel is nearly equal to that for bulk

water, suggesting that  $\text{H}_2\text{O}$  molecules in gel are in the same chemical environment as in bulk water, and as such the effect of structurally ordered  $\text{H}_2\text{O}$  near mineral surfaces is probably negligible. This occurs as a result of the large population of unbound  $\text{H}_2\text{O}$  far from the grain surface compared to the small population of bound  $\text{H}_2\text{O}$  in water-rich gels. (3) The contribution of bound  $\text{H}_2\text{O}$  can be elucidated from Figure 4 as follows. The  $\text{I}^-$  may be excluded from the interlamellar space of mica platelets because of the electrostatic expulsion between  $\text{I}^-$  and the negatively charged grain surface. This is undesirable because it limits the effectiveness of  $\text{I}^-$  for probing the entire geometrical complexity of the gel. However, the effect is negligible for the low-density water-rich gels used in the present study (Madsen, 1998). Hence, the diffusion of  $\text{I}^-$  is free from chemical interactions (anion exclusion) with the grain surface; it is governed only by the geometrical complexity of the pore structure. As a result, the contribution from the geometrical tortuosity is  $1 - D^{\text{iodine}}/D_0^{\text{iodine}}$  and that from the less mobile or bound  $\text{H}_2\text{O}$  is  $D^{\text{iodine}}/D_0^{\text{iodine}} - D^{\text{water}}/D_0^{\text{water}}$ . Although there are small fluctuations, Figure 4 shows that  $D^{\text{iodine}}/D_0^{\text{iodine}} - D^{\text{water}}/D_0^{\text{water}}$  is negligible when compared with  $1 - D^{\text{iodine}}/D_0^{\text{iodine}}$ . On the basis of the above (points 1–3), the contribution of bound  $\text{H}_2\text{O}$  to the average diffusivity measured by PGSE NMR is negligible for  $w$  of <24.8 wt.% mica gels. Free or unbound  $\text{H}_2\text{O}$  molecules diffuse in the geometrically complex and tortuous pore structure of mica-mineral grains. The principal reason for the decrease in  $\text{H}_2\text{O}$  diffusivity (equation 5) is therefore, the geometrical complexity of the porous media.

#### Montmorillonite gel

The results of the X-ray CT analysis of montmorillonite gels are listed in Table 3. The experimental procedure was the same as that for mica gels. Filter paper saturated with dense KI solution was placed on the gel at  $t = 0$  s. The resultant diffusive migration of iodine from the filter paper was imaged by X-ray CT. Profile

averages, similar to those for Figure 5b, were taken to improve the signal-to-noise ratio.  $D^{\text{iodine}}$  was calculated by fitting equation 4 to the averaged profile. An average of values taken over a number of CT snapshots is listed in Table 3.

A discussion similar to that for mica gels is possible regarding the contribution of bound  $\text{H}_2\text{O}$  molecules to the average diffusivity.  $\text{H}_2\text{O}$  molecules migrate long distances [ $(6\Delta D^{\text{water}})^{1/2} = 6\text{--}43 \mu\text{m}$ ] and are thus affected by the complex pore structure of the gel. The value of  $E$  for montmorillonite gel is nearly equal to that for bulk water (Nakashima, 2001a). The normalized diffusivities of  $\text{H}_2\text{O}$  and  $\text{I}^-$  are shown in Figure 6. There is a suggestion of a weak contribution from bound  $\text{H}_2\text{O}$  as indicated by the slightly higher  $D^{\text{iodine}}/D_0^{\text{iodine}}$  than  $D^{\text{water}}/D_0^{\text{water}}$ . However, because  $D^{\text{iodine}}/D_0^{\text{iodine}} - D^{\text{water}}/D_0^{\text{water}}$  is much smaller than  $1 - D^{\text{iodine}}/D_0^{\text{iodine}}$ , bound  $\text{H}_2\text{O}$  molecules do not play important roles for  $w < 16.7$  wt.% montmorillonite.

We therefore propose a microstructure model linking to the argument on Na-rich montmorillonite put forth by Ichikawa *et al.* (1999). Figure 7 is a pore-geometry model relating  $w$  to the pore-size,  $d$ . Discoidal clay platelets (thickness  $a$  and radius  $r$ ) are scattered randomly in the gel. There are bound or hydrated  $\text{H}_2\text{O}$  layers near the negatively charged clay grains (Duval *et al.*, 1999). If the number density of the platelets is  $n$ , then  $d \approx (1/n)^{1/3}$ . It is then straightforward to derive that  $n = \rho_{\text{bulk}} w / (100\rho_{\text{clay}}\pi r^2 a)$  where  $\rho_{\text{clay}}$  is the density of montmorillonite grains,  $r = 400 \text{ nm}$  (Monma *et al.*, 1997), and  $\rho_{\text{bulk}}$  is given in Table 1 of Nakashima (2001a). It is reasonable to assume that  $a = 1 \text{ nm}$  and

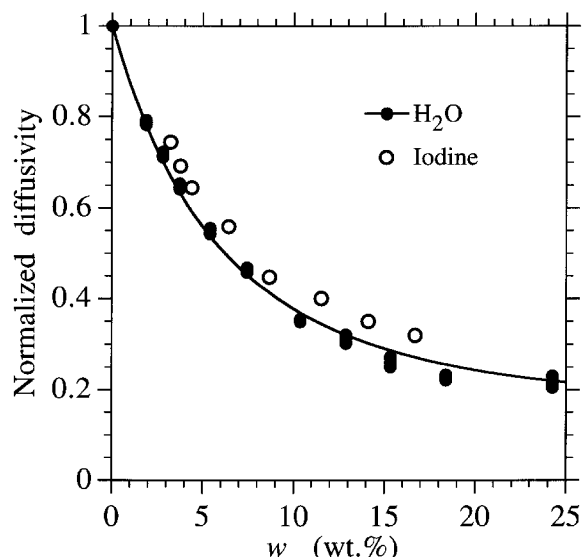


Figure 6. Normalized iodine-diffusivity,  $D^{\text{iodine}}/D_0^{\text{iodine}}$ , vs. montmorillonite fraction,  $w$  (data from Table 3). Normalized  $\text{H}_2\text{O}$ -diffusivity,  $D^{\text{water}}/D_0^{\text{water}}$ , for 30.4, 39.5, 50.5 and 60.0°C is also given (data from Nakashima, 2001a).  $\text{H}_2\text{O}$  diffusivity data are fitted to equation 5 giving  $\alpha = 1.77$  and  $\beta = 0.0798$ .

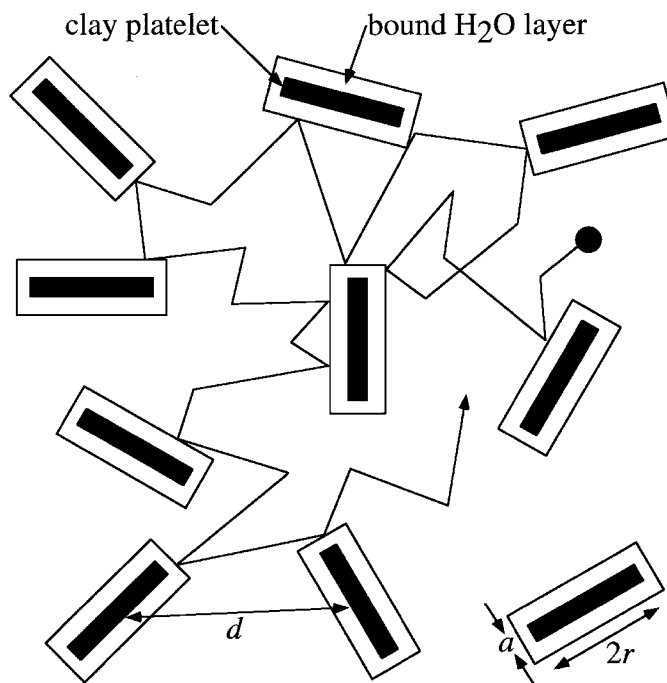


Figure 7. Schematic microstructure of montmorillonite gel. Solid clay platelets (thickness  $a$  and radius  $r$ ) are scattered randomly. The pore-size or average distance between clay platelets is  $d$ . An example of the random walk trajectory of unbound  $H_2O$  or  $I^-$  (solid circle) diffusing and avoiding obstacles (clay platelets with hydrated water layers) is also shown.

$\rho_{\text{clay}} = 2.6 \text{ g/cm}^3$ . As a result,  $d \approx 410 \text{ nm}$  for  $w = 1.9 \text{ wt.\%}$  and  $d \approx 180 \text{ nm}$  for  $w = 18.4 \text{ wt.\%}$ . Ichikawa *et al.* (1999) predicted that  $H_2O$  molecules of only 3 to 4 nm thickness near the negatively charged Na-rich montmorillonite surfaces were bound or less mobile in terms of diffusivity. The pore-size of the gels is  $d = 180\text{--}410 \text{ nm}$  in the present study, which is much larger than 3–4 nm. This calculation suggests that the population of free  $H_2O$  is much larger than that of bound  $H_2O$ . Thus it is reasonable that the effect of bound  $H_2O$  on the average diffusivity of the gel system is almost negligible for montmorillonite gels of  $< 18 \text{ wt.\%}$  (Figure 6). These conclusions are consistent with the prediction by Ichikawa *et al.* (1999).

## CONCLUSIONS

It has been shown that the effect of bound  $H_2O$  is almost negligible for mica- and clay-gel systems of  $> \sim 80 \text{ wt.\%}$   $H_2O$  in terms of the average  $H_2O$  diffusivity of the systems. This is attributable to the large population of unbound  $H_2O$  far from the grain surface compared to the small population of bound  $H_2O$  near the grain surface. Although the effects may be also negligible for other water-rich smectite gels, the applicability to other clays requires further study. The PGSE NMR coupled with X-ray CT has been shown to be a useful tool for determining the effect of bound  $H_2O$  on the average self-diffusivity in water-rich gels.

## ACKNOWLEDGMENTS

The author would like to thank C.A. Weiss, A. Caprihan and D.C. Bain for their helpful comments. The author is also grateful to Y. Kanai for the use of the centrifuge and to Y. Nakashima for help with the NMR experiments. The public domain NIH Image program (developed at the US National Institutes of Health and available on the Internet at <http://rsb.info.nih.gov/nih-image/>) was used in the X-ray CT image analysis. Samples of ME-100 were provided by CO-OP Chemical Co., Ltd. (URL = <http://www.jade.dti.ne.jp/~coopchem/>). A 60 MHz proton NMR spectrometer, MY60FT (JEOL, Tokyo, Japan), without gradient coils at the Geological Survey of Japan was used for the preliminary experiments. This study was supported by a grant from the Ministry of Education, Culture, Sports, Science and Technology of Japan.

## REFERENCES

- Callaghan, P.T. (1991) *Principles of Nuclear Magnetic Resonance Microscopy*. Oxford University Press, Oxford, UK, 492 pp.
- Cebula, D.J., Thomas, R.K. and White, J.W. (1981) Diffusion of water in Li montmorillonite studied by quasielastic neutron scattering. *Clays and Clay Minerals*, **29**, 241–248.
- Chang, F.-R.C., Skipper, N.T. and Sposito, G. (1995) Computer simulation of interlayer molecular structure in sodium montmorillonite hydrates. *Langmuir*, **11**, 2734–2741.
- Crank, J. (1975) *The Mathematics of Diffusion*. Oxford University Press, Oxford, UK, 414 pp.
- Denison, C., Carlson, W.D. and Ketcham, R.A. (1997) Three-dimensional quantitative textural analysis of metamorphic rocks using high-resolution computed X-ray tomography:

- Part I. methods and techniques. *Journal of Metamorphic Geology*, **15**, 29–44.
- Duliu, O.G. (1999) Computer axial tomography in geosciences: an overview. *Earth Science Reviews*, **48**, 265–281.
- Duval, F.P., Porion, P. and Damme, H.V. (1999) Microscale and macroscale diffusion of water in colloidal gels. A pulsed field gradient and NMR imaging investigation. *Journal of Physical Chemistry B*, **103**, 5730–5735.
- Fripiat, J.J., Letellier, M. and Levitz, P. (1984) Interaction of water with clay surfaces. *Philosophical Transactions of the Royal Society of London*, **A311**, 287–299.
- Furusawa, T. (1997) Synthesis and utilization of clay minerals. *Journal of Clay Science Society of Japan*, **37**, 112–117 (in Japanese with English abstract).
- Ichikawa, Y., Kawamura, K., Nakano, M., Kitayama, K. and Kawamura, H. (1999) Unified molecular dynamics and homogenization analysis for bentonite behavior: Current results and future possibilities. *Engineering Geology*, **54**, 21–31.
- Johnson, C.S., Jr. (1996) Diffusion measurements by magnetic field gradient method. Pp. 1626–1644 in: *Encyclopedia of Nuclear Magnetic Resonance* (D.M. Grant and R.K. Harris, editors). John Wiley & Sons, New York.
- Kita, H., Iwai, T. and Nakashima, S. (1989) Diffusion coefficient measurement of an ion in pore water of granite and tuff. *Journal of Japan Society of Engineering Geology*, **30**, 26–32 (in Japanese with English abstract).
- Kleinberg, R.L. and Vinegar, H.J. (1996) NMR properties of reservoir fluids. *The Log Analyst*, **37**, 20–32.
- Krynicki, K., Green, C.D. and Sawyer, D.W. (1979) Pressure and temperature dependence of self-diffusion in water. *Faraday Discussions of the Chemical Society*, **66**, 199–208.
- Latour, L.L., Kleinberg, R.L., Mitra, P.P. and Sotak, C.H. (1995) Pore-size distributions and tortuosity in heterogeneous porous media. *Journal of Magnetic Resonance*, **A112**, 83–91.
- Lerman, A. (1979) *Geochemical Processes: Water and Sediment Environments*. Wiley, New York, 481 pp.
- MacGillavry, C.H. and Rieck, G.D. (1962) *International Tables for X-ray Crystallography* (Vol. III, *Physical and Chemical Tables*). The Kynoch Press, Birmingham, UK, 362 pp.
- Madsen, F.T. (1998) Clay mineralogical investigations related to nuclear waste disposal. *Clay Minerals*, **33**, 109–129.
- McBride, M.B. (1994) Mobility of small molecules in interlayers of hectorite gels: ESR study with an uncharged spin probe. *Clays and Clay Minerals*, **42**, 455–461.
- Mills, R. (1973) Self-diffusion in normal and heavy water in the range 1–45°. *Journal of Physical Chemistry*, **77**, 685–688.
- Monma, T., Kudo, M. and Masuko, T. (1997) Flow behaviors of smectite/water suspensions in terms of particle-coagulated structures. *Journal of Clay Science Society of Japan*, **37**, 47–57 (in Japanese with English abstract).
- Nakashima, S. (1995) Diffusivity of ions in pore water as a quantitative basis for rock deformation rate estimates. *Tectonophysics*, **245**, 185–203.
- Nakashima, Y. (2000a) The use of X-ray CT to measure diffusion coefficients of heavy ions in water-saturated porous media. *Engineering Geology*, **56**, 11–17.
- Nakashima, Y. (2000b) Effects of clay fraction and temperature on the H<sub>2</sub>O self-diffusivity in hectorite gel: A pulsed-field-gradient spin-echo nuclear magnetic resonance study. *Clays and Clay Minerals*, **48**, 603–609.
- Nakashima, Y. (2001a) Pulsed field gradient proton NMR study of the self-diffusion of H<sub>2</sub>O in montmorillonite gel: Effects of temperature and water fraction. *American Mineralogist*, **86**, 132–138.
- Nakashima, Y. (2001b) Pulsed-gradient spin-echo NMR study of the H<sub>2</sub>O self-diffusivity in clay gels. *Magnetic Resonance Imaging*, **19**, 579.
- Nakashima, Y., Hirai, H., Koishikawa, A. and Ohtani, T. (1997) Three-dimensional imaging of arrays of fluid inclusions in fluorite by high-resolution X-ray CT. *Neues Jahrbuch für Mineralogie, Monatshefte*, December, 559–568.
- Nakashima, Y., Mitsumori, F., Nakashima, S. and Takahashi, M. (1999) Measurement of self-diffusion coefficients of water in smectite by stimulated echo <sup>1</sup>H nuclear magnetic resonance imaging. *Applied Clay Science*, **14**, 59–68.
- Ohtani, T., Nakano, T., Nakashima, Y. and Muraoka, H. (2001) Three-dimensional shape analysis of miarolitic cavities and enclaves in granite by an X-ray computed tomography. *Journal of Structural Geology*, **23**, 1741–1751.
- Olson, E.A., Han, K.S. and Pisano, D.J. (1981) CT reprojection polychromaticity correction for three attenuators. *IEEE Transactions on Nuclear Science*, **28**, 3628–3640.
- Stejskal, E.O. and Tanner, J.E. (1965) Spin diffusion measurements: Spin echos in the presence of a time-dependent field gradient. *Journal of Chemical Physics*, **42**, 288–292.
- Tateyama, H., Nishimura, S., Tsunematsu, K., Jinnai, K., Adachi, Y. and Kimura, M. (1992) Synthesis of expandable fluorine mica from talc. *Clays and Clay Minerals*, **40**, 180–185.
- Tuck, J.J., Hall, P.L. and Hayes, M.H. (1985) Quasi-elastic neutron-scattering studies of intercalated molecules in charge-deficient layer silicates: Part 2 – High resolution measurements of the diffusion of water in montmorillonite and vermiculite. *Journal of the Chemical Society Faraday Transactions 1*, **81**, 833–846.
- van Geet, M., Swennen, R. and Wevers, M. (2000) Quantitative analysis of reservoir rocks by microfocus X-ray computerized tomography. *Sedimentary Geology*, **132**, 25–36.
- Wellington, S.L. and Vinegar, H.J. (1987) X-ray Computerized Tomography. *Journal of Petroleum Technology*, August, 885–898.
- Yu, J.W. and Neretnieks, I. (1997) Diffusion and sorption properties of radionuclides in compacted bentonite. *SKB Technical Report* (Swedish Nuclear Fuel and Waste Management Co.), **97-12**, 1–98.

(Received 18 January 2001; revised 8 May 2001; Ms. 513)